Quasielastic scattering of ^{6}He from ^{12}C at 82.3 MeV/nucleon

J. L. Lou(楼建玲), Y. L. Ye(叶沿林),* D. Y. Pang(庞丹阳), Z. X. Cao(曹中鑫), D. X. Jiang(江栋兴), T. Zheng(郑涛), H. Hua(华辉), Z. H. Li(李智焕), X. Q. Li(李湘庆), Y. C. Ge(葛愉成), L. H. Lv(吕林辉), J. Xiao(肖军), Q. T. Li(李奇特), R. Qiao(乔锐), H. B. You(游海波), and R. J. Chen(陈瑞九)
School of Physics and State Key Laboratory of Nuclear Physics and Technology, Peking University, Beijing 100871, China

H. Sakurai, H. Otsu, M. Nishimura, S. Sakaguchi, H. Baba, Y. Togano, K. Yoneda, C. Li(李琛), S. Wang(王硕), H. Wang(王赫), and K. A. Li(李阔昂)
RIKEN, 2-1Hirosawa, Wako, Saitama 351-0198, Japan

T. Nakamura, Y. Nakayama, Y. Kondo, and S. Deguchi
Department of Physics, Tokyo Institute of Technology, Tokyo 152-8551, Japan

Y. Satou and K. Tshoo
Department of Physics and Astronomy, Seoul National University, 599 Gwanak, Seoul 151-742, Korea
(Received 29 December 2010; published 23 March 2011)

Quasielastic scattering of ^{6}He on a ^{12}C target was measured at 82.3 MeV/nucleon. Special care was taken to treat the background subtraction at very small angles. The measured differential cross-sections show a large enhancement at small angles relative to the Rutherford cross-section, similar to those observed at lower energies for the scattering of halo nuclei. The overall structure of the cross-section is reasonably reproduced by the optical model calculations. The inelastic channels which populate two low-lying excited states of ^{12}C target nucleus were included in the framework of the coupled channel analysis. Further systematic theoretical analysis is encouraged.

DOI: 10.1103/PhysRevC.83.034612 PACS number(s): 25.60.Bx, 25.70.Bc, 24.10.−i

I. INTRODUCTION

Elastic scattering is known as the most fundamental and simplest process accompanying the hadronic collision between any pair of projectile and target [1]. The optical potential (OP) obtained from the elastic scattering is not only important in itself to represent the global effective interaction between the colliding partners, but also necessary for describing the entrance and exit channel potentials for more complicated reaction processes, such as fusion, breakup, few-nucleon transfer, and so on. Therefore soon after the advent of exotic structures of unstable nuclei, such as nuclear halo or skin, elastic scattering has become one of the most intensively studied collision channels induced by radioactive ion beams [2,3]. The exotic properties of an unstable nucleus are often related to its small binding energy and large extent of the matter density distribution [4]. When this kind of nucleus is elastically scattered by a target, couplings to other nonelastic channels are expected to be much stronger in comparison to the scattering induced by a tightly bound nucleus, and the corresponding OPs should exhibit some new characteristics [1].

Within the framework of Feshbach theory [5], OP can be written in a form of $U = V + U_{\rm pol}$, where V is a real potential corresponding to the ground-state scattering only, and $U_{\rm pol}$ is a complex, nonlocal and energy-dependent potential arising from couplings to all nonelastic channels, including excitation of particle-bound states or resonant states of the projectile or target, direct breakup to the continuum, transfer of nucleons, and so on. In principle, $U_{\rm pol}$, known as the dynamic polarization potential (DPP), is composed of a real part ($V_{\rm pol}$) and an imaginary part ($W_{\rm pol}$). But deeply bound nuclei couplings to nonelastic channels are weak, and $U_{\rm pol}$ could simply be represented by an imaginary term with a form similar to that of the real potential V, with the latter being calculated by some microscopic folding methods or obtained phenomenologically by fitting to experimental data [1]. For loosely bound nuclei, especially halo nuclei, couplings to breakup and transfer channels may be strong, and explicit treatments of both the $V_{\rm pol}$ and the $W_{\rm pol}$ are necessary. At first it was realized that the scattering of loosely bound nuclei from the hydrogen target could be described by using an OP with a reduction of the depth of its real part and eventually an enhancement of its imaginary part, relative to the potential for a deeply bound nucleus [1,6–8]. This renormalization is a reminiscence of the DPP effect. For scattering from a complex target (a carbon target, for instance), this renormalization method is not good enough, and an appropriate $V_{\rm pol}$ should be applied that modifies the shape of the real potential at the surface region [7,9,10]. Sometimes similar modification is also needed for the imaginary potential [10]. Of course, it would be better to treat the couplings explicitly through coupled channel methods, such as the coupled reaction channel model, which deals with specific inelastic excitations or transfer processes [11–13], and the continuum discretized coupling channel (CDCC) model, which incorporates the effect of breakup to continuum [14–16]. But inclusion of every new channel requires a number of inputs such as spectroscopic factors and OP parameters, etc., which may not be available in the literature. Also the assumption of few-body structure and

*yeyl@pku.edu.cn

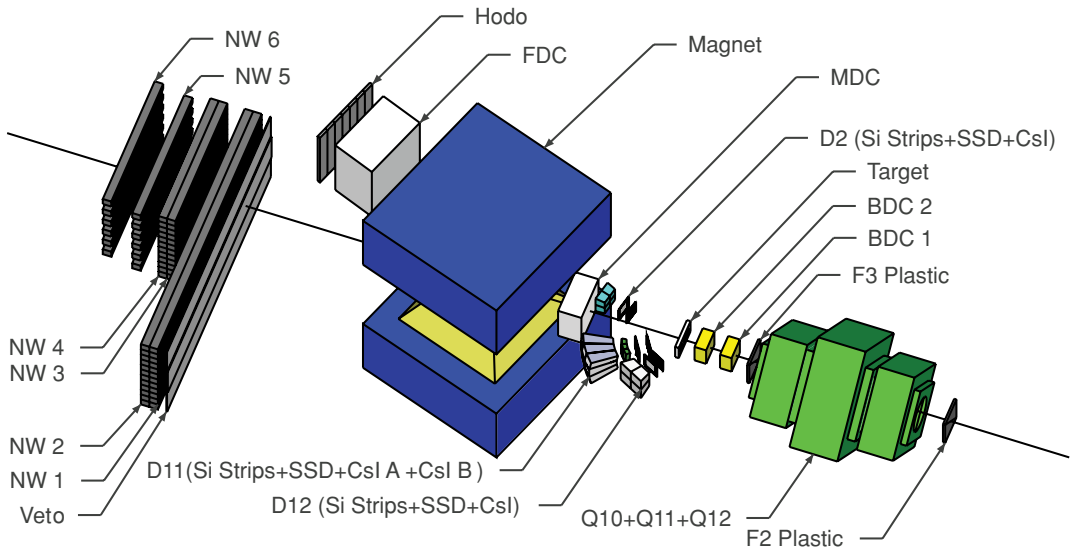

FIG. 1. (Color online) Schematic view of the experimental setup at RIKEN-RIPS.

the related treatment necessary for the CDCC calculation is applicable only for some selected systems. As a result the phenomenological DPP is still useful in many cases [15]. Efforts have also been made to deduce the DPP theoretically from the CDCC S matrix or within the semiclassical approach [17] in order to understand its behavior for various systems at different energies. Despite much progress made over the last two decades, strong coupling effects for loosely bound exotic nucleus remain central problems for current and future nuclear physics with unstable nucleus beams.

On the experimental side, some elastic scattering differential cross-sections for weakly bound light exotic nuclei, such as ^{6}He, ^{8}He, ^{11}Li, and $^{10-12,14}$Be, have been measured and well tabulated in Ref. [2]. These measurements were concentrated at energies below 50 MeV/nucleon, except for a couple early works for ^{11}Li, ^{12,14}Be, and ^{8}He at about 60 MeV/nucleon and using simple 0° particle telescopes [18–21]. We note that these early measurements suffered from some experimental uncertainties for very small angle measurements, especially when extremely exotic nuclei like ^{11}Li, ^{14}Be, and ^{8}He were concerned. As a matter of fact, the secondary radioactive beam has an inevitably large beam spot and angular spread, which affect the small angle measurement. Also the tracking detectors installed just in front of the target would create some background scattering in addition to the scattering from the physical target. This situation is very different from measurements with stable nucleus beams and must be treated very carefully. The key point is to subtract correctly the overwhelmingly large target-out background at small angles.

^{6}He is the lightest halo nucleus with a small binding energy (0.97 MeV) and no particle-bound excited state. It should be a good test case to study coupling effects, especially the coupling to continuum states. A systematic investigation of ^{6}He elastic scattering at about 38 MeV/nucleon on proton and carbon targets has been carried out at GANIL [6,9], and very interesting information related to DPP was extracted. Many other experiments for ^{6}He scattering were performed at lower energies [2], whereas data at higher energies are scarce. We report here the quasielastic scattering of ^{6}He at 82.3 MeV/nucleon on a ^{12}C target. Detailed description of the experiment is given in Sec. II, including a special treatment of small angle data. Optical model (OM) analysis was performed and is described in Sec. III.

II. EXPERIMENT

The experiment was carried out at the RIKEN projectile fragment separator (RIPS) radioactive ion beam line [22]. The main goal of the experiment was to study the knockout reaction mechanism [23], but quasielastic scattering data were acquired automatically and are presented in this article. A schematic view of the experimental setup is given in Fig. 1. The secondary beam of ^{6}He at 82.3 MeV/nucleon was produced from a 115 MeV/u ^{13}C primary beam impinged on a ^{9}Be target with a thickness of 12 mm. The beam intensity at the physical target position amounts to 3×10^{5} pps with a purity of 85% for ^{6}He. The contaminations, mainly ^{3}H and ^{8}Li, can be eliminated through offline data analysis by applying cuts on the time of flight(TOF) between the plastic scintillation counters at focus points F2 (F2 plastic) and F3 (F3 plastic), and the energy loss (ΔE) in a F2 plastic scintillator. A CH_2 foil with a thickness of 83 mg/cm^2 and a carbon film with a thickness of 133.9 mg/cm^2 were mounted as the physical targets. Since the beam spot on the target is relatively large, two beam-tracking drift chambers, BDC1 and BDC2 [24], were placed at 572.5 and 193.5 mm upstream from the target in order to determine the incident angle event by event. The position resolution of the BDCs is smaller than 0.5 mm, corresponding to an incident angle resolution of less than 0.1°. During the offline data analysis a cut on the projected beam spot at the target position was applied.

A deflection magnet was employed downstream of the target in order to keep the forward neutron wall away from being exposed to the direct beam. The combined multitrack

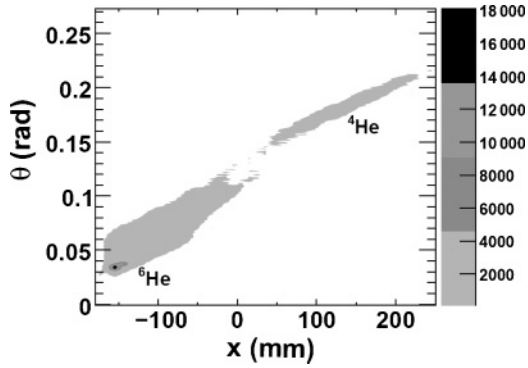

FIG. 2. Charged particle identification for outgoing fragments at around 0°, determined by the magnet system. x and θ are horizontal positions and relative deflection angles measured by the FDC.

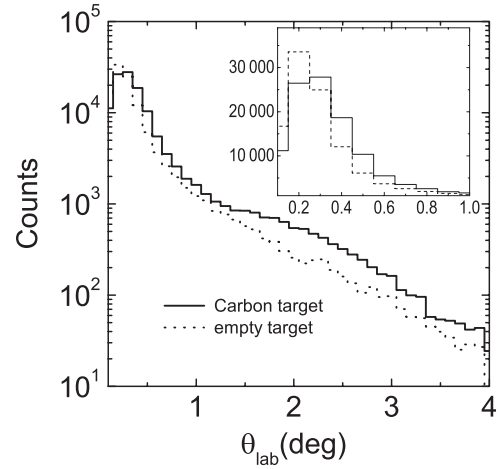

FIG. 3. Angular distributions of the scattered ^{6}He particles from carbon target and empty target, respectively, which are normalized to the same number of incident particles. The inset in the right upper corner is a linear display for very small angles.

drift chamber (MDC) [25–27] and fragment drift chamber (FDC) [24], which were installed at the entrance and exit sides of the magnet, respectively, provided tracking information for scattered ^{6}He and breakup fragments within 4.0°(laboratory system) relative to the the beam axis. A hodoscope wall composed of seven plastic scintillation bars (HODO) was placed at the exit of the FDC in order to measure the TOF and energy loss of the fragments. Each bar has a size of 450 mm (height) × 100 mm (width) × 5 mm (thickness) and is coupled to two photomultiplier tubes at both ends. Bars 1 and 2 of HODO were directly hit by the main ^{6}He beam and were eliminated from the event trigger.

In order to detect the fragments at larger angles, a particle telescope D2, covering an angular range from 5° to 19° (laboratory system) for setup 1 and from 7° to 21° for setup 2, was installed at a distance of 337 mm from the target. D2 is composed of one double-sided silicon strip detector (DSSSD) 1 mm in thickness and 64 × 64 mm^2 in area, one large surface silicon detector (SSD) 1.5 mm in thickness, and one thick layer of CsI(Tl) crystal with four sectors. The strip width of the DSSSD is 2 mm at both sides. Two other telescopes, D11 and D12, installed at the other side of the beam axis, were especially designed to detect the recoiled protons, which are useful for selecting the knockout reaction mechanism [23] but are of no concern for the current elastic scattering data analysis.

For fragments deflected by the magnet, the particle identification may be obtained by using the measured horizontal position in the FDC (x) and the track deflection angle relative to the FDC central axis (θ), as shown in Fig. 2.

For very small angle scattering it is important to correctly define the zero-degree line (z axis) for the whole detection system since the yield at a small angle changes rapidly, and a small angular deviation could lead to a remarkable error for the scattering cross-section value [28]. When preparing the experimental setup, we align the whole detection system mechanically, which may bring about an uncertainty of millimeters. Therefore, for offline data analysis we correct this alignment by using the actual beam with an empty target (target out). In this way, the z axis is fixed by the beam itself, independent of the manual operation. This approach allows us to limit the absolute uncertainty of the z axis to be less than 0.1° [28]. Scattering angles can then be calculated event by event from incident tracks determined by the BDCs and outgoing tracks determined by the target hit positions and the MDC positions. Figure 3 shows the experimental angular distribution of the scattered ^{6}He particles for carbon and empty targets, respectively, normalized to the same number of incident particles. It is interesting to see directly that the effect of the target is to remove some of beam particles (flux) from a very small angular region to a little larger angular region, and the crossover of the relative number of particles appears at about 0.3°, as shown in the inset picture of the figure. Considering the position resolution of MDC (less than 0.5 mm) and the distance between the target and the MDC (553 mm), the angular resolution is deduced to be less than 0.2° (FWHM), including contributions from the uncertainties of the incident direction and the multiple Coulomb scattering of the projectile in the target. The angular bin is then selected as 0.5° for each data point in the laboratory system, considering the angular resolution and the event statistics. At very small angles, counting rates induced by the direct beam with the empty target are very large, and the spectrum tail can extend to a few degrees, as shown in Fig. 3. But reliable scattering data still can be obtained for scattering angles larger than 0.5°, where the difference between target-in and target-out data is at least three times larger than the fluctuations of the spectrum (square root of the counting number for each bin), and therefore the subtraction of the latter from the former is reliable [28]. It should be noted that enough counting time for empty target runs is mandatory in order to get a statistically stable background spectrum, which in turn ensures a good subtraction. As indicated in Sec. I, we consider the careful treatment of the 0° axis alignment and the background subtraction at small angles very important for a scattering experiment with the secondary unstable nucleus beam.

The detection solid angle for each data point was deduced from a Monte Carlo simulation calculation, which took into account the angular distribution of the incident beam and the actual geometry of the detector setup. The comparison between the MDC position spectrum shape with and without

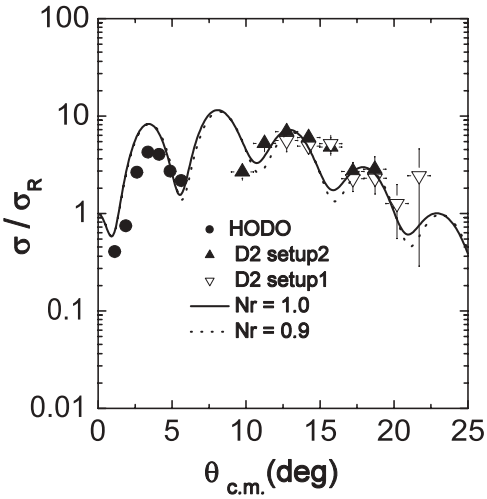

FIG. 4. Differential cross-sections as the ratio to Rutherford cross-sections for ^{6}He quasielastic scattering from the carbon target at 82.3 MeV/nucleon. The points are experimental data measured by the magnet system (solid circles) and by the D2 telescope (triangles). The solid and dotted lines are from the OM calculations with parameter sets A and B in Table I, respectively.

the coincidence with the HODO scintillation counters allows us to verify that it is the frame of D2 telescope and the edge of the first triggered HODO scintillator bar (bar 3) that limit the acceptance. In the simulation the detection system acceptance was defined accordingly.

For each angular bin the number of scattered ^{6}He from the pure carbon target is obtained by subtracting the target-out contribution from the target-in count, normalized to the same number of incident particles. Finally differential cross-sections as the ratio to Rutherford cross-sections are presented in Fig. 4 as the seven solid circles up to 5.62° in the center-of-mass (c.m.) system.

To extend the experimental data to larger angles, events detected by the D2 telescope for a carbon target and empty target were also analyzed. As an example, Fig. 5 depicts the particle identification performance of the D2 telescope, obtained by plotting the energy loss in the SSD versus the stopping energy in one of the CsI(Tl) crystals. The ^{6}He component is clearly separated in the figure. The scattering angle for each event is now determined by the position on the DSSSD, together with the incident track information provided by the BDCs. The angular resolution is less than 0.5° in the laboratory system, deduced from the position resolution of the detector and the related distance to the target. Considering the data statistic, the angular bin is selected to be 1° in the laboratory system.

Figure 6 presents a typical total energy spectrum of ^{6}He detected by the D2 telescope with the empty target background subtracted. In principle, the total energy is a sum of the deposit energy in the CsI(Tl) crystal and the energy loss in the thin silicon detector layers (1 mm thick DSSSD and 1.5 mm thick SSD). The energy loss in 2.5 mm silicon is almost a constant for ^{6}He with energy of a few tens of MeV per nucleon and takes only a very small portion of the total energy (about 2.6 MeV/u compared to about 80 MeV/u). In addition

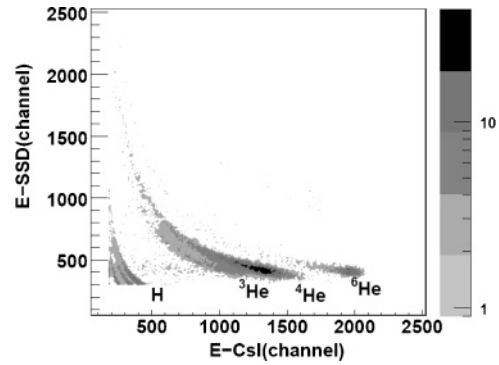

FIG. 5. Particle identification spectrum obtained from the D2 telescope, illustrated by the energy loss in the SSD versus the stopping energy in one of the CsI(Tl) crystals.

the straggling of the energy loss is negligibly small (about 0.076 MeV/u) in comparison to the energy spread caused by the energy resolution of the CsI(Tl) crystal (about 5% FWHM) and has no influence on the energy spectrum shape. Therefore we simply add an estimated constant energy loss into the measured deposit energy in the CsI(Tl) crystal and build the spectrum as shown in Fig. 6. In the spectrum a high-energy peak corresponding to the quasielastically scattered ^{6}He stands out clearly. The peak counting can be obtained from the integral of the Gaussian function, which fits fairly well the high-energy side of the experimental spectrum [28]. Due to the limited energy resolution (about 5% FWHM), the peak counting should incorporate the contribution from the inelastic scattering, which excites ^{12}C target, although the ^{6}He projectile has no bound excited state. In the figure two considered states (see also Sec. III B) at excitation energies of 4.44 and 9.65 MeV, respectively, are indicated by the arrows. These states will be treated in the following theoretical calculations. The single-proton separation threshold of ^{12}C is also shown

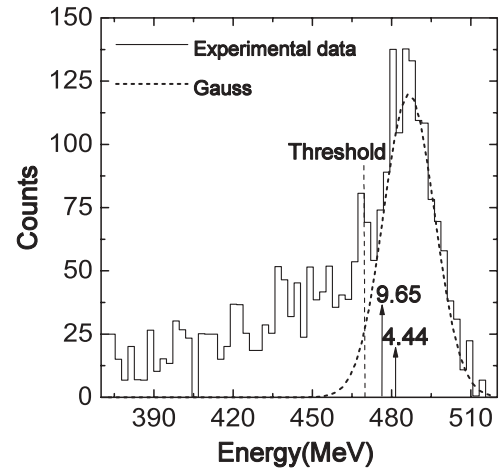

FIG. 6. ^{6}He energy spectrum detected by the D2 telescope. A Gaussian peak function (dashed curve) is used to fit the high-energy side of the spectrum. The numbers (4.44 and 9.65) denote the excitation energies (in MeV) of the considered states in the ^{12}C target. The vertical dashed line indicates the one-proton separation threshold for ^{12}C.

by the vertical dashed line. It seems that the low-energy "tail" of the spectrum comes mostly from the target breakup process, but it affects the quasielastic peak slightly when the high-energy side fitting procedure was applied.

Again, the solid angle corresponding to each angular bin is deduced from Monte Carlo simulation. In total seven experimental data points for setup 2 (solid triangles in Fig. 4) and seven data points for setup 1 (empty triangles) were obtained, extending the experimental differential cross-sections up to 21.7° in the c.m. system. The excellent agreement of the independent data points for the two setups in the overlap angular region demonstrates the good treatment of the peak fitting and solid angle simulation. The error bars in Fig. 4 are statistical only, resulting from the number of incident and scattered ^{6}He and the background subtraction. In addition some 12% systematic error is estimated to result mainly from the uncertainties of target thickness, selection of elastic peak, and simulation of the solid angle.

The measured differential cross-sections in Fig. 4 exhibit a large enhancement relative to the Rutherford cross-section at small angles, which is comparable to what was observed at other incident energies for halo nuclei [9,18,21].

III. THEORETICAL ANALYSIS

A. OM analysis with semimicroscopic potentials

The experimental data were analyzed in the framework of the OM by using the code FRESCO [29]. The OP is expressed in the form

$$U(r) = N_r \times V_F(r) + iW(r) + V_C(r). \quad (1)$$

The real potential $V_F(r)$ is calculated by the microscopic double-folding method [30]. As in Ref. [9], we adopt the CDM3Y6 nucleon-nucleon (NN) interaction, a halo-type matter distribution ($fc6$) for ^{6}He, and a two-parameter Fermi function distribution for ^{12}C. N_r is the renormalization factor of the real potential. $W(r)$ is the imaginary potential of a standard Wood-Saxon (WS) form with three parameters W, R_w, and a_w for the depth, radius, and diffuseness, respectively. The reduced radius r_w is related to R_w as $r_w = R_w/(A_p^{1/3} + A_t^{1/3})$, where A_p and A_t are mass numbers of the projectile and the target, respectively. $V_C(r)$ is the Coulomb potential corresponding to a uniformly distributed charge sphere with a radius $R_c = r_c(A_p^{1/3} + A_t^{1/3})$ for $r_c = 1.2$ fm. In total four parameters, N_r, W, R_w (or r_w), and a_w, could be adjusted in order to fit experimental data.

At first, we fix $N_r = 1.0$ and search for the three parameters W, r_w, and a_w. Since the reasonable fitting could be achieved only with r_w value close to 1, we simply keep it at 0.97 fm, the same as that in Ref. [9]. The optimal values for W and a_w are then obtained as listed in Table I (set A), and the corresponding angular distribution is drawn as the solid curve in Fig. 4. The amplitudes at larger angles and the oscillatory structure at small angles of the experimental differential cross-sections are reasonably reproduced by the calculation. However, the amplitude of the peak at about 3° and the minimum at around 9° are not described in a quantitative way. It was indicated that for the scattering of a light loosely bound nucleus the real folding potential should be reduced by a small fraction [31,32]. For instance, $N_r = 0.9$ was adopted for ^{6}He + ^{12}C scattering at 38.3 MeV/nucleon [9]. We tried this renormalization procedure but could not find obvious improvement. An example for $N_r = 0.9$ is shown in Fig. 4 by the dotted line, with the corresponding optimized imaginary potential parameters listed in Table I (set B). More attempts were made to improve the description of experimental data by adjusting N_r, W, $R_w(r_w)$, and a_w at the same time, but no qualitative improvement could be achieved. The total reaction cross-sections corresponding to the above OP are also presented in the table, which are consistent with those obtained at other energies [9].

TABLE I. Optimized OP parameters for ^{6}He + ^{12}C system at an incident energy of 82.3 MeV/nucleon.

Set	N_r	W MeV	r_w fm	a_w fm	σ_r mb
A	1.0	62.77	0.97	0.50	853
B	0.9	59.61	0.97	0.48	828

B. Effects of inelastic channels

As pointed above, the experimental data presented in Fig. 4 include contributions from inelastic excitations of the carbon target, due to the limited energy resolution. These contributions could be accounted for by coupled channel calculations. Excitations of the first 2^+ (4.44 MeV) and 3^- (9.64 MeV) states of ^{12}C were taken into consideration in the calculations since they are known to have the largest inelastic scattering cross-sections for the ^{12}C target at various energies [20,21,33,34]. The first 0^+(7.65 MeV) excited state also lies within the experimental energy resolution. However, as a monopole excitation, it is not expected to be strongly populated in an inelastic scattering process and is normally ignored [20,21,33,34]. We use the rotational model of ^{12}C with

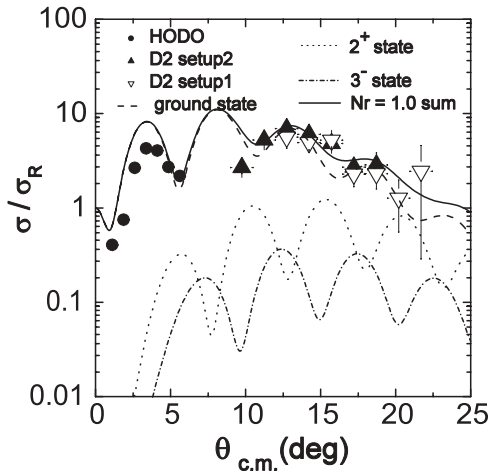

FIG. 7. OM calculations of the differential cross-sections for ^{6}He + ^{12}C scattering at 82.3 MeV/nucleon, including the contributions from the inelastic channels as described in the text.

deformation lengths $\delta_2 = 1.08$ fm for transition to the 2^+ state and $\delta_3 = 0.67$ fm for transition to the 3^- state, respectively. These parameters were taken from Ref. [35]. We did not make much effort to optimize the deformation parameters since the contribution of the inelastic channels affects only the differential cross-sections at large angles where the structure is less pronounced and changes of the amplitudes could easily be compensated by the adjustment of the OP parameters. Fits to experimental data including contributions from these inelastic channels were performed, and the result is presented in Fig. 7. The OP parameters of set A do not need to be changed for the optimum fit, but the total reaction cross-section is reduced from 853 to 843 mb. It can be seen that the effect of the 2^+ state is negligible for CM angles smaller than 10°, and its relative contribution increases to about 30% above 15°. Contributions from the 3^- state are much smaller and can be neglected for the whole angular range covered by the current measurement.

Again, the amplitude of the oscillation at small angles cannot be reproduced quantitatively by OM calculations that include the inelastic channels. This kind of discrepancy was also found for scattering of other loosely bound nuclei [7,18,19,21], especially at higher incident energies. It is suggested that, especially for the scattering of the halo nucleus, coupling to a breakup channel should be taken into account through the inclusion of phenomenological DPP or the explicit coupled channel treatment in the framework of CDCC [15,16]. We leave this to future work since the incorporation of target excitation channels is still difficult for the current CDCC code.

IV. SUMMARY

Quasielastic scattering of ^{6}He on a ^{12}C target was measured at 82.3 MeV/nucleon. The upstream and downstream drift chambers allowed us to determine the scattering angle accurately. At very small angles the background subtraction was performed with a special effort. The measured differential cross-sections show a large enhancement at small angles relative to the Rutherford cross-section, similar to those observed at lower energies for the scattering of halo nuclei.

The overall structure of the cross-section is reasonably reproduced by a semimicroscopical OM calculation applying a set of OP parameters consistent with those obtained at lower energies. Furthermore the inelastic channels corresponding to two low-lying excited states of ^{12}C target nucleus were included in the framework of coupled channel analysis. Further systematic theoretical analysis with the phenomenological DPP potentials or with the CDCC method, by taking into account all existing experimental data at around the present energy [18–21], is certainly encouraged.

ACKNOWLEDGMENTS

We are very grateful to the staffs of the Ring Cyclotron in RIKEN who provided the high-quality ^{13}C beam and the staff of the RIPS-Lab and Tokyo Institute of Technology for their hospitality and technical support. DYP gives his special thanks to Dao T. Khoa for providing the double-folding code DFPD2. This work is supported by the National Basic Research Program of China (No. 2007CB815002), the National Natural Science Foundation of China (Nos. 11035001, 10775003, 10821140159, 10905002), the China Postdoctoral Science Foundation (No. 20100470133), the Grant-in-Aid for Scientific Research (No. 15740145) of MEXT Japan, and the WCU program (No. R32-2008-000-10155-0) of NRF Korea.

[1] M. Brandan and G. Satchler, Phys. Rep **285**, 143 (1997).
[2] N. Keeley, N. Alamanos, K. W. Kemper, and K. Rusek, Prog. Part. Nucl. Phys. **63**, 396 (2009).
[3] A. DiPietro *et al.*, Phys. Rev. Lett **105**, 022701 (2010).
[4] S. N. Ershov, L. V. Grigorenko, J. S. Vaagen, and M. V. Zhukov, J. Phys. G: Nucl. Part. Phys. **37**, 064026 (2010).
[5] H. Feshbach, Ann. Phys. **5**, 357 (1958).
[6] V. Lapoux *et al.*, Phys. Lett. B **517**, 18 (2001).
[7] V. Lapoux *et al.*, Phys. Lett. B **658**, 198 (2008).
[8] F. Jamil-Qureshi *et al.*, Chin. Phys. Lett. **27**, 092501 (2010).
[9] V. Lapoux *et al.*, Phys. Rev. C **66**, 034608 (2002).
[10] M. Y. M. Hassan, M. Y. H. Farag, E. H. Esmael, and H. M. Maridi, Phys. Rev. C **79**, 064608 (2009).
[11] G. R. Satchler, *Direct Nuclear Reactions* (Clarendon Press, Oxford, 1983).
[12] I. J. Thompson, Comput. Phys. Rep. **7**, 167 (1989).
[13] R. S. Mackintosh and N. Keeley, Phys. Rev. C **81**, 034612 (2010).
[14] N. Austern, Y. Iseri, M. Kamimura, M. Kawai, G. Rawitscher, and M. Yahiro, Phys. Rep. **151**, 125 (1987).
[15] K. Rusek, K. W. Kemper, and R. Wolski, Phys. Rev. C **64**, 044602 (2001).
[16] A. M. Moro, K. Rusek, J. M. Arias, J. Gomez-Camacho, and M. Rodriguez-Gallardo, Phys. Rev. C **75**, 064607 (2007).
[17] R. S. Mackintosh and N. Keeley, Phys. Rev. C **79**, 014611 (2009).
[18] J. J. Kolata *et al.*, Phys. Rev. Lett. **69**, 2631 (1992).
[19] M. Zahar *et al.*, Phys. Rev. C **49**, 1540 (1994).
[20] M. Zahar *et al.*, Phys. Rev. C **54**, 1262 (1996).
[21] J. A. Tostevin *et al.*, Phys. Rev. C **56**, R2929 (1997).
[22] T. Kubo *et al.*, Nucl. Instrum. Methods Phys. Res. Sect. B **70**, 309 (1992).
[23] Y. Ye *et al.*, Nucl. Phys. A **834**, 454C (2010).
[24] T. Nakamura *et al.*, Phys. Rev. Lett. **96**, 252502 (2006).
[25] Y. Satou *et al.*, Phys. Lett. B **660**, 320 (2008).
[26] Y. Kondo *et al.*, Phys. Rev. C **79**, 014602 (2009).
[27] Y. Kondo *et al.*, Physics. Lett. B **690**, 245 (2010).
[28] Y. L. Ye *et al.*, Phys. Rev. C **71**, 014604 (2005).
[29] I. J. Thompson, Comput. Phys. Rep. **7**, 167 (1988).
[30] D. T. Khoa and G. R. Satchler, Nucl. Phys. A **668**, 3 (2000); D. T. Khoa, DFPD2 code (unpublished).
[31] N. Alamanos and P. Roussel-Chomaz, Ann. Phys. (Paris) **21**, 601 (1996).
[32] D. T. Khoa, G. R. Satchler, and W. von Oertzen, Phys. Rev. C **51**, 2069 (1995).
[33] J. S. Al-Khalili, I. J. Thompson, and J. A. Tostevin, Nucl. Phys. A **581**, 331 (1995).
[34] I. Pecina *et al.*, Phys. Rev. C **52**, 191 (1995).
[35] A. Kiss, C. Mayer-Boricke, M. Rogge, P. Turek, and S. Wiktor, J. Phys. G **13**, 1067 (1987).